

# ChemComm

Chemical Communications

Accepted Manuscript

This article can be cited before page numbers have been issued, to do this please use: V. Y. Shevtsov, F. gambino, D. R. Nosov, J. Guillot, S. Porporato, G. A. Elia, C. Gerbaldi and A. S. Shaplov, *Chem. Commun.*, 2026, DOI: 10.1039/D6CC00051G.



This is an Accepted Manuscript, which has been through the Royal Society of Chemistry peer review process and has been accepted for publication.

Accepted Manuscripts are published online shortly after acceptance, before technical editing, formatting and proof reading. Using this free service, authors can make their results available to the community, in citable form, before we publish the edited article. We will replace this Accepted Manuscript with the edited and formatted Advance Article as soon as it is available.

You can find more information about Accepted Manuscripts in the [Information for Authors](#).

Please note that technical editing may introduce minor changes to the text and/or graphics, which may alter content. The journal's standard [Terms & Conditions](#) and the [Ethical guidelines](#) still apply. In no event shall the Royal Society of Chemistry be held responsible for any errors or omissions in this Accepted Manuscript or any consequences arising from the use of any information it contains.

# Low Melting Non-corrosive Asymmetric Thioether-TFSI Li Salts for Solid Polymer Electrolytes†

DOI: 10.1039/D6CC00051G

Received 00th January 20xx,  
Accepted 00th January 20xxVladislav Y. Shevtsov,<sup>ab‡</sup> Francesco Gambino,<sup>cd‡</sup> Daniil R. Nosov,<sup>a</sup> Jérôme Guillot,<sup>e</sup> Silvia Porporato,<sup>cd</sup> Giuseppe A. Elia<sup>cd</sup>, Claudio Gerbaldi,<sup>cd\*</sup> and Alexander S. Shaplov<sup>a\*</sup>

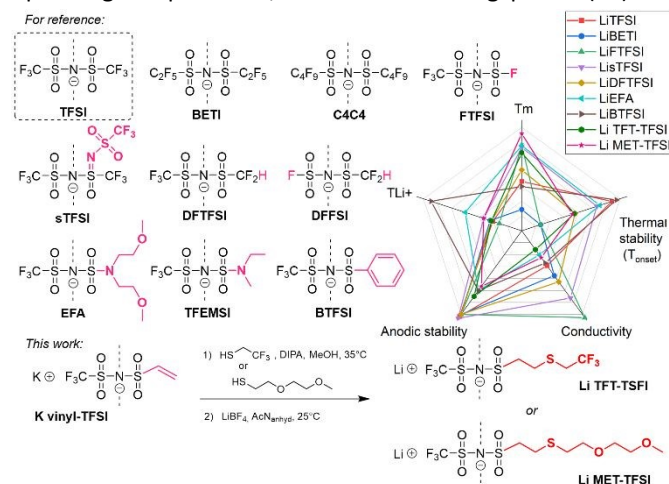
DOI: 10.1039/x0xx00000x

High crystallinity in poly(ethylene oxide) (PEO)-based solid polymer electrolytes (SPEs) limits ionic transport, electrochemical stability, and the operating temperature range of Li-metal batteries. Herein, two asymmetric, low-melting thioether-TFSI lithium salts were synthesized via a modular thiol-ene strategy and incorporated into PEO-based SPEs. Their pronounced plasticizing effect efficiently suppresses PEO crystallinity while preserving ionic conductivity, Li<sup>+</sup> transference, and electrochemical stability. In addition, both SPEs mitigate aluminum current-collector corrosion by forming a stable passivation layer, addressing a key limitation of conventional LiTFSI systems. As a result, the SPEs exhibit improved compatibility with Li metal and enable stable cycling of Li||LiFePO<sub>4</sub> cells with high capacity retention and coulombic efficiency.

The market for portable electronics, including mobile phones, laptops, and remotely operated devices, is increasingly dominated by lithium-ion (Li-ion) and lithium-polymer (Li-Po) batteries based on liquid organic electrolytes. In contrast, lithium metal polymer (LiMP) batteries employ solid polymer electrolytes (SPEs), typically prepared by dissolving a Li salt in a polymer matrix, most commonly poly(ethylene oxide) (PEO). SPEs offer several advantages, including higher energy density, greater freedom in battery size, shape, and flexibility, and improved safety due to the absence or strongly reduced content of flammable organic solvents or plasticizers.<sup>1</sup>

Because safety is critical for market deployment, a major breakthrough was the introduction of lithium bis(trifluoromethylsulfonyl)imide (LiTFSI, Scheme 1), featuring a weakly coordinating, highly charge-delocalized TFSI<sup>-</sup> anion.<sup>2</sup> Weak coordination enhances Li<sup>+</sup> mobility, enabling high ionic conductivity (3.9×10<sup>-4</sup> S cm<sup>-1</sup> at 70°C,<sup>3</sup> the typical operating temperature of LiMP batteries), together with excellent thermal and chemical stability, prompting efforts to replace the less

thermally stable and more hazardous LiPF<sub>6</sub>.<sup>3-5</sup> However, LiTFSI exhibits several well-known drawbacks in PEO-based SPEs (Table 1), including a low Li<sup>+</sup> transference number ( $T_{Li^+} = 0.22$ ),<sup>6</sup> lower ionic conductivity than LiPF<sub>6</sub>/PEO systems,<sup>7</sup> poor long-term interfacial stability toward Li metal due to unstable SEI formation, and pronounced corrosion of aluminum current collectors.<sup>4,8</sup> These limitations have driven intensive research into TFSI<sup>-</sup> anion modification and the development of new weakly coordinating anions to achieve higher ionic conductivity, improved Li-anode interfacial stability, and better cycling performance with aluminum current collectors.<sup>6,9-12</sup> One promising strategy involves Li salts that are liquid at battery operating temperatures, as reduced melting points ( $T_m$ ) can



plasticize the PEO matrix, suppress crystallization, and broaden the operational temperature window of SPEs.

**Scheme 1** TFSI and asymmetric derivatives: reference structures and synthesis of thioether-TFSI Li salts.

Early studies in this field examined how the length and symmetry of fluoroalkyl chains in TFSI-like anions affect the properties of Li salts and their SPEs (Scheme 1; e.g., LiBETI,<sup>13</sup> LiFTFSI,<sup>6</sup> LiC4C4,<sup>14</sup> LiC1C4,<sup>15</sup> etc.). Increasing perfluoroalkyl chain length (LiTFSI-LiBETI-LiC4C4) was shown to improve SPE interfacial compatibility with both anode and cathode materials (Table 1)<sup>14</sup>. However, this modification increased  $T_m$  of salts melting points, exerted opposing effects on ionic conductivity of Li salt/PEO materials, and does not enhance Li<sup>+</sup> transport, as highly fluorinated groups interact only weakly with PEG chains.<sup>6,13,14,16</sup> In contrast, introducing asymmetry into the TFSI anion substantially reduces  $T_m$  while improving other SPE properties.<sup>17-20</sup> Consequently, recent research has focused on asymmetric

<sup>a</sup> Functional Polymeric and Particulate Materials Unit, Luxembourg Institute of Science and Technology (LIST), 28 avenue des Hauts-Fourneaux, L-4362 Esch-sur-Alzette, Luxembourg.

<sup>b</sup> Department of Physics and Materials Science, University of Luxembourg, L-4365 Esch-sur-Alzette, Luxembourg.

<sup>c</sup> GAME Lab, Department of Applied Science and Technology (DISAT), Politecnico di Torino, 24 Corso Duca degli Abruzzi, 10129 Torino, Italy.

<sup>d</sup> National Reference Center for Electrochemical Energy Storage (GISEL), 9 Via G. Giusti, 50121 Firenze, Italy

<sup>e</sup> Advanced Analyses and Support Unit, Luxembourg Institute of Science and Technology (LIST), 28 avenue des Hauts-Fourneaux, L-4362 Esch-sur-Alzette, Luxembourg.

† Electronic supplementary information (ESI) available. See DOI: 10.1039/x0xx00000x

‡ V.Y.S and F.G. contributed equally to this work.



weakly coordinating anions, with several TFSI-type systems showing attractive features (Scheme 1). Lithium super-TFSI (**sTFSI**<sup>17,18</sup>) exhibits a markedly lower melting point (118 °C<sup>18</sup> vs. 233 °C for **LiTFSI**). This reduction, together with enhanced salt solubility, allows PEO SPEs to achieve approximately doubled ionic conductivity at 70 °C and a slightly increased  $T_{Li^+}$  without compromising electrochemical stability (Table 1).<sup>18</sup> However, stable cycling of Li||LiFePO<sub>4</sub> cells with **LiTFSI** has been demonstrated only in ionic liquid (IL) electrolytes, requiring combination with ILs such as [N-alkyl-N-methylpiperidinium<sup>+</sup> sTFSI].<sup>21</sup>

Building on anion asymmetry, several studies introduced a positive dipole into the anion structure, leading to **DFTFSI**<sup>7,20,22</sup> and **DFFSI**<sup>19</sup> anions, where one fluorine atom was replaced by hydrogen. This modification caused only a modest reduction in  $T_m$  of Li-salt; however, **LiDFTFSI/PEO**<sup>20</sup> and **LiDFFSI/PEO**<sup>19</sup> SPEs showed ~1.5 fold higher ionic conductivity than **LiTFSI/PEO**, reduced interfacial resistance, improved compatibility with metal Li, and strongly suppressed Al corrosion. **LiDFTFSI/PEO**<sup>20</sup> exhibited increased  $T_{Li^+}$  (0.22 to 0.35), attributed to -CF<sub>2</sub>H... PEO hydrogen bonding. As a result, **LiDFFSI/PEO** enabled Li||LiFePO<sub>4</sub> cycling at 70 °C for up to 125 cycles at C/10,<sup>19</sup> while **LiDFTFSI/PEO**, benefiting from higher anodic stability, supported Li||Li-S cells at similar rates, albeit with capacity fading.<sup>22</sup>

A related strategy combining anion asymmetry with stronger polymer interactions was applied in **EFA**<sup>23</sup> and **TFEMSI**<sup>24</sup> anions, where a tertiary amine is directly attached to the sulfonyl group. Incorporation of short PEG chains lowers the  $T_m$  of **LiEFA** to 112 °C (Table 1) and increases the  $T_{Li^+}$  to 0.43 via segmental entanglement and hydrogen bonding with PEO.<sup>23</sup> However, this design reduced electrochemical stability toward Li (~4 V) and slightly lowered thermal stability.<sup>23</sup> Nevertheless, **LiEFA/PEO** SPEs enabled stable Li<sup>o</sup>||LiFePO<sub>4</sub> cycling for 30 cycles at C/3, attributed to (i) suppressed anion mobility, reducing concentration polarization and dendrite formation, and (ii) formation of a stable SEI that facilitates Li<sup>+</sup> transport across the interface.

To date, one of the highest Li<sup>+</sup> transference numbers reported for PEO-based SPEs ( $T_{Li^+}$  = 0.69) has been achieved using **LiBTFSI**.<sup>25</sup> This high selectivity was attributed to  $\pi$ - $\pi$  stacking between anion-attached benzene rings, promoting anion self-aggregation and suppressing negative-charge mobility. While the total ionic conductivity of **LiBTFSI/PEO** is comparable to **LiTFSI/PEO**, its anodic stability is reduced to ~4.0 V, and aluminum corrosion was not evaluated.<sup>25</sup> Nevertheless, the SPE showed excellent compatibility with Li metal, enabling stable solid-state Li<sup>o</sup>||LiFePO<sub>4</sub> cycling with 86% capacity retention after 200 cycles at C/3 rate.

Despite these advances and other strategies, such as the incorporation of fillers<sup>26,27</sup>, simultaneously improving ionic conductivity in PEO-based SPEs and mitigating interfacial instability in LiMP batteries remains challenging, as gains often compromise Li<sup>+</sup> selectivity, thermal and electrochemical stability, moisture resistance, or aluminum compatibility. Moreover, reducing fluorine content in Li salts is increasingly important for large-scale deployment and regulatory compliance. To address the need for non-corrosive lithium salts with weakly coordinating anions, low  $T_m$ , and SPEs combining high ionic conductivity with elevated  $T_{Li^+}$ , we developed a simple

synthetic strategy based on thiol-ene click chemistry (Scheme 1).<sup>28</sup> This approach uses commercially available potassium vinyl-TFSI<sup>29</sup> and enables modular access to a broad family of asymmetric anions through a two-step reaction with selected thiols. The method features operational simplicity, consistently high yields, facile product isolation, and high purity suitable for electrochemical applications.

**Table 1** Thermal and electrochemical properties of Li salts and respective Li salt/PEO SPEs

Li salt	Neat Li salt		Li salt/PEO polyelectrolyte <sup>a</sup>		
	$T_m^b$ (°C)	$T_{onset}^c$ (°C)	$\sigma$ 70°C (S cm <sup>-1</sup> )	LSV <sup>d</sup> 70°C (V)	$T_{Li^+}^e$ 70°C
<b>Li TFT-TFSI</b>	136	240	$2.1 \times 10^{-4}$	4.4	0.23
<b>Li MET-TFSI</b>	71	235	$3.0 \times 10^{-4}$	4.1	0.29
For comparison:					
<b>Li TFSI</b> <sup>6,14</sup>	233	356	$3.9 \times 10^{-4}$	4.6-5.1	0.22
<b>Li BETI</b> <sup>13</sup>	328	<i>n.d.</i>	$5.0 \times 10^{-4}$	<i>n.d.</i>	0.24
<b>Li C<sub>4</sub></b> <sup>14</sup>	352	334	$2.2 \times 10^{-4}$	5.3	0.29
<b>Li FTFSI</b> <sup>6</sup>	110	150	$9.7 \times 10^{-4}$	5.2	0.17
<b>Li sTFSI</b> <sup>18</sup>	118	300	$7.5 \times 10^{-4}$	5.4	0.29
<b>Li DFFSI</b> <sup>19</sup>	<i>n.d.</i>	184	$6.6 \times 10^{-4}$	<i>n.d.</i>	0.23
<b>Li DFTFSI</b> <sup>20</sup>	194	242	$5.7 \times 10^{-4}$	5.2	0.35
<b>Li EFA</b> <sup>23</sup>	112	308	$2.7 \times 10^{-4}$	4.0	0.43
<b>Li TFEMSI</b> <sup>24</sup>	181	318	$3.5 \times 10^{-4}$	<i>n.d.</i>	0.64
<b>Li BTFSI</b> <sup>11,25</sup>	<i>n.d.</i>	352	$3.6 \times 10^{-4}$	4.0	0.69

<sup>a</sup> The Li salts/PEO blends composition was fixed at [EO]/[Li<sup>+</sup>]=20 (note: PEO with different molecular weights may be used). <sup>b</sup> Melting point ( $T_m$ ) determined by DSC under N<sub>2</sub> (note: heating rates of 5 or 10°C min<sup>-1</sup> may be employed). <sup>c</sup> Onset weight loss temperature determined by TGA in air (note: heating rates of 5 or 10°C min<sup>-1</sup> may be employed). <sup>d</sup> Anodic stability by linear sweep voltammetry (LSV) at 70°C. <sup>e</sup> Li-ion transference number measured at 70°C.

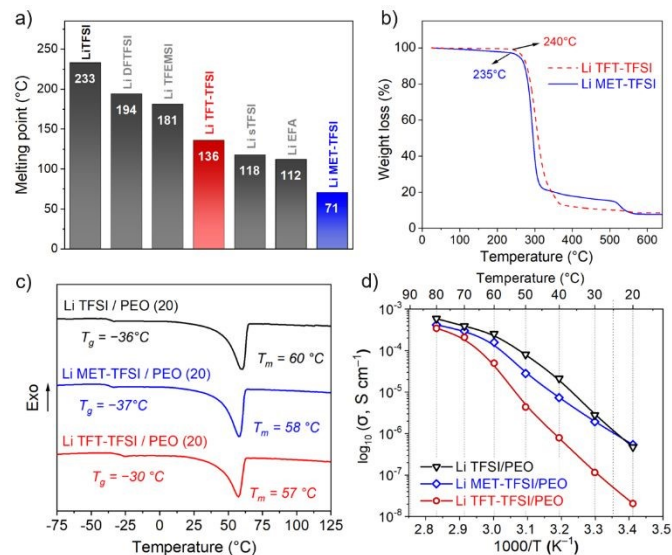
In this work, **vinyl-TFSI K** was reacted with 2,2,2-trifluoroethanethiol and 2-(2-methoxyethoxy)ethane-1-thiol (Scheme 1). The former affords a minimal asymmetric anion bearing a fluorinated -CH<sub>2</sub>-CF<sub>3</sub> group, while the latter introduces two ethylene oxide units expected to interact with PEO and reduce anion mobility. Subsequent cation exchange yielded the target thioether-TFSI lithium salts: lithium ((2-((2,2,2-trifluoroethyl)thio)ethyl)sulfonyl)-N-(trifluoromethylsulfonyl)-imide (**Li TFT-TFSI**) and lithium ((2-((2-(2-methoxyethoxy)ethyl)thio)ethyl)sulfonyl)-N-(trifluoromethylsulfonyl)imide (**Li MET-TFSI**). Structural integrity and purity were confirmed by <sup>1</sup>H, <sup>7</sup>Li, <sup>13</sup>C and <sup>19</sup>F NMR, IR spectroscopy, and elemental analysis (Fig. S1-S11, ESI<sup>†</sup>). 2D NMR experiments (HSQC, HMBC) enabled full proton and carbon assignment of **Li MET-TFSI** (Fig. S12-S13, ESI<sup>†</sup>).

Differential scanning calorimetry (DSC) showed melting points ( $T_m$ , observed during the first heating) of 136 and 71 °C for **Li TFT-TFSI** and **Li MET-TFSI**, respectively (Fig. S14-S15, ESI<sup>†</sup>), with the latter representing the lowest  $T_m$  reported for TFSI-type Li salts to date (Fig. 1a). This strong melting-point reduction is attributed to the methoxyethoxy-thioethyl substituent, whose steric and conformational effects disrupt anion packing and suppress crystallization. Consistently, the second DSC cycle



showed no crystallization upon slow cooling and only a glass transition ( $T_g \approx -3.0$  °C) was detected. Thermogravimetric analysis (TGA) in air revealed an onset of weight loss above 235 °C (Fig. 1b), indicating sufficient thermal stability for practical application, as LiMP batteries typically operate below 100 °C.

**Fig. 1** Physical, thermal, and electrochemical properties of neat Li salts and Li<sub>x</sub>/PEO



polyelectrolytes ( $X = \text{TFT-TFSI}$ ,  $\text{MET-TFSI}$ , or  $\text{TFSI}$ ;  $[\text{EO}/\text{Li}^+] = 20$ ): a) Summary of melting points of asymmetric sulfonimide Li salts; b) TGA plots of neat Li salts in air; c) DSC traces of polyelectrolytes; d) Arrhenius plots of ionic conductivity vs. inverse temperature for polyelectrolytes determined by EIS in the range 20–80 °C.

Converting the Li salts into PEO-based SPEs with an  $[\text{EO}]/[\text{Li}^+]$  ratio of 20 yielded self-standing, semi-transparent membranes, whose thermal properties were analyzed by DSC (Fig. 1c and Fig. S16–S17, ESI<sup>†</sup>). Figure 1c shows first-heating DSC traces of Li TFT-TFSI/PEO and Li MET-TFSI/PEO SPEs, benchmarked against LiTFSI/PEO. All samples exhibited a glass transition ( $T_g = -37.4$  to  $-29.6$  °C) and a PEO melting transition ( $T_m = 57.3$ – $60.5$  °C). The  $T_g$  values decrease in the order:  $-29.6$  °C (Li TFT-TFSI/PEO) >  $-35.7$  °C (LiTFSI/PEO) >  $-37.4$  °C (Li MET-TFSI/PEO), indicating a stronger plasticizing effect of Li MET-TFSI. Analysis of the melting transition showed  $T_m$  values of  $60.5$  °C (LiTFSI/PEO) >  $58.0$  °C (Li MET-TFSI/PEO) >  $57.3$  °C (Li TFT-TFSI/PEO), consistent with melting enthalpies  $\Delta H_m$  of 68.5, 66.2, and 54.1 J g<sup>-1</sup>, respectively. These results demonstrate reduced PEO crystallinity in Li MET-TFSI/PEO and Li TFT-TFSI/PEO compared to LiTFSI/PEO. This reduction arises from both the lower intrinsic melting points of the new salts and their enhanced plasticizing efficiency. Additionally, suppressed PEO recrystallization can be attributed to the increased flexibility and larger substituents of the modified TFSI anions<sup>6,18,22</sup>, which enhance segmental mobility and hinder crystallization.

Figure 1d presents Arrhenius plots of total ionic conductivity ( $\sigma$ ), reflecting combined Li<sup>+</sup> and anion transport, for Li TFT-TFSI/PEO, Li MET-TFSI/PEO, and LiTFSI/PEO SPEs. In the near-ambient range (20–30 °C), Li MET-TFSI/PEO shows the highest conductivity ( $5.4 \times 10^{-7}$  S cm<sup>-1</sup>), exceeding LiTFSI/PEO ( $4.7 \times 10^{-7}$  S cm<sup>-1</sup>) and Li TFT-TFSI/PEO ( $2.0 \times 10^{-8}$  S cm<sup>-1</sup>). However, conductivities of all systems remain insufficient for LiMP batteries, mainly due to crystalline PEO domains that strongly

impede ion transport. Upon heating above 60 °C, conductivity increased sharply for all SPEs, reaching  $2.0 \times 10^{-5}$  S cm<sup>-1</sup> (Fig. 1d), attributed to melting-induced amorphization of the PEO matrix that enables continuous ion-conducting pathways and enhances ion mobility.<sup>1</sup> At 70 °C, ionic conductivity increased with decreasing effective anion volume in the order (Table 1):  $2.1 \times 10^{-4}$  S cm<sup>-1</sup> (Li TFT-TFSI/PEO) <  $3.0 \times 10^{-4}$  S cm<sup>-1</sup> (Li MET-TFSI/PEO)  $\leq 3.9 \times 10^{-4}$  S cm<sup>-1</sup> (LiTFSI/PEO).

To evaluate the suitability of thioether-TFSI lithium salts for application in LiMP batteries, the electrochemical properties of Li TFT-TFSI/PEO and Li MET-TFSI/PEO were systematically investigated with particular attention to the  $\text{T}_{\text{Li}^+}$ , anodic stability, compatibility with the Li metal electrode, and cycling performance in Li<sup>o</sup> Li<sub>x</sub>/PEO LiFePO<sub>4</sub> (LFP) cells. The Li-ion transference number of the SPEs was determined using the Evans–Vincent–Bruce method (Fig. S18). Notably, Li MET-TFSI/PEO exhibited a higher  $\text{T}_{\text{Li}^+}$  value (0.29) compared to LiTFSI/PEO (0.22) and Li TFT-TFSI/PEO (0.23). This enhanced  $\text{T}_{\text{Li}^+}$  can be attributed to a combination of two effects: (i) increased mobility of Li<sup>+</sup>-containing species resulting from the lower  $T_g$  of the SPE, enabled by the stronger plasticizing effect of Li MET-TFSI, and (ii) reduced mobility of the MET-TFSI anions due to their stronger interactions with the PEO matrix.

The linear sweep voltammograms (LSVs) of the SPEs are compared in Fig. 2a. All SPEs show anodic breakdown at  $\sim 4$  V vs. Li/Li<sup>+</sup>, attributed to oxidative degradation of the PEO matrix.<sup>30</sup> Increasing the potential to  $\sim 4.8$  V resulted in a sharp rise in polarization current, indicating the onset of oxidative decomposition involving the thioether anions, possibly together with PEO. The oxidative stability of the Li salt/PEO blends at 70 °C follows the trend: Li TFSI (LSV = 4.6 V) > Li TFT-TFSI (4.4 V) > Li MET-TFSI (4.1 V). Nonetheless, both newly developed Li salts exhibit sufficient anodic stability for operation in LFP batteries. Anodic dissolution tests were performed using 1 M Li salt solutions in EC/DMC (1:1 v/v) with uncoated Al discs by holding the potential 1.3 V above the open-circuit potential of the corresponding half-cell (Fig. S19, ESI<sup>†</sup>). During first cycle, current densities of  $\sim 0.9$  and  $\sim 0.1$   $\mu\text{A}$  were recorded for Li MET-TFSI and Li TFT-TFSI, which are negligible compared to LiTFSI, for which a sustained current density of  $\sim 15$  mA cm<sup>-2</sup> was observed (Fig. S19). This pronounced response for LiTFSI clearly indicates anodic dissolution of the Al<sup>o</sup> current collector.<sup>7</sup> In contrast, the very low currents for Li MET-TFSI and Li TFT-TFSI are attributed to the formation of a highly resistive passivation layer on the Al surface, effectively suppressing anodic dissolution.<sup>7,31,32</sup> XPS analysis revealed increased Li- and F-rich species on Al after anodic dissolution in Li MET-TFSI and Li TFT-TFSI electrolytes, compared to LiTFSI (Fig. S20–S21), indicating a more fluoride-rich interphase with higher LiF and AlF<sub>3</sub> content and improved corrosion protection (see ESI<sup>†</sup>). Strongly reduced corrosion was further confirmed by FESEM: severe pitting was observed for LiTFSI after cycling (Fig. S22, ESI<sup>†</sup>),<sup>31</sup> whereas no pitting features were detected on Al discs from Li MET-TFSI or Li TFT-TFSI electrolytes (Figs. S23–S24, ESI<sup>†</sup>). Figure 2b shows the discharge capacity as a function of current density (C/20, C/15, C/10, C/5, and back to C/15) for Li<sup>o</sup> Li<sub>x</sub>/PEO LiFePO<sub>4</sub> cells. SPEs based on Li TFT-TFSI and Li MET-TFSI display stable



charge/discharge behavior across all C-rates, together with excellent cycling stability and high Coulombic efficiency. Both SPEs maintain capacities close to the theoretical value of  $\text{LiFePO}_4$  ( $\approx 160 \text{ mAh g}^{-1}$ ), with Coulombic efficiencies above 98% at all tested rates (Figs. 2b and S25–S27, ESI<sup>†</sup>), whereas the conventional **LiTFSI/PEO** electrolyte delivers significantly lower capacities of  $\sim 130$ – $140 \text{ mAh g}^{-1}$  under identical conditions (Fig. S28–S29, ESI<sup>†</sup>). Figure 2c presents galvanostatic lithium plating/stripping in  $\text{Li}^0$  symmetric cells at  $70^\circ\text{C}$  and different current densities. While **LiTFSI/PEO** exhibits pronounced voltage instabilities already at  $0.1 \text{ mA cm}^{-2}$ , the TFT-TFSI- and MET-TFSI-based SPEs allow stable cycling at  $0.2 \text{ mA cm}^{-2}$  with lower overpotentials than the reference system. During long-term cycling at  $0.05 \text{ mA cm}^{-2}$  (Fig. 2d), the **Li TFT-TFSI/PEO** and **Li MET-TFSI/PEO** cells remained stable for over 600 h, whereas the **LiTFSI**-based cell short-circuited after  $\sim 250$  h, indicating markedly improved  $\text{Li}^0$  electrode stability due to reduced concentration polarization and suppressed dendritic lithium growth. Moreover, **Li TFT-TFSI** and **Li MET-TFSI** SPEs sustain higher current densities compared to **LiTFSI/PEO** that short-circuits rapidly, as indicated by CCD tests (Fig. S30, ESI<sup>†</sup>).

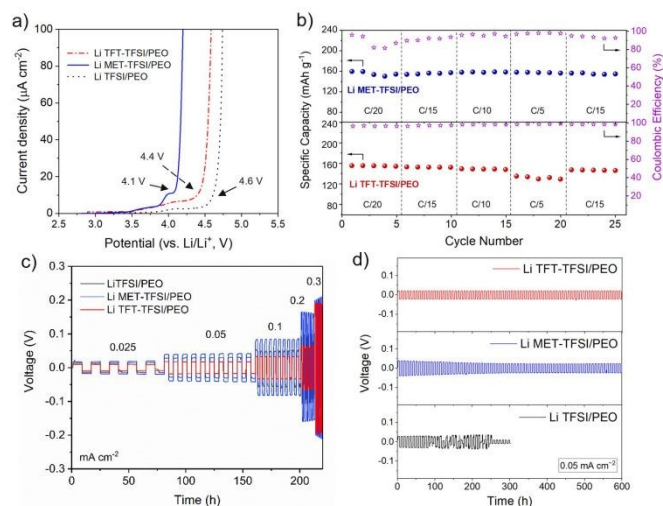


**Fig. 2** Electrochemical behavior of **Li TFT-TFSI/PEO** (red), **Li MET-TFSI/PEO** (blue), and **Li TFSI/PEO** (black) at  $70^\circ\text{C}$ : a) linear sweeping voltammetry profiles measured in a  $\text{Li}^0$   $\text{Li}_x/\text{PEO}$  Al carbon-coated configuration at a scan rate of  $0.1 \text{ mV s}^{-1}$ ; b) specific capacity and coulombic efficiency as a function of cycle number for  $\text{Li}^0$   $\text{Li}_x/\text{PEO}$   $\text{LiFePO}_4$  cells at variable C-rates; c) galvanostatic cycling of  $\text{Li}^0$   $\text{Li}_x/\text{PEO}$   $\text{Li}^0$  symmetric cells at different current densities (total plated/stripped capacity of  $0.3 \text{ mAh cm}^{-2}$  per half cycle); d) long-term cycling performances of  $\text{Li}$  symmetric cell at  $0.050 \text{ mA cm}^{-2}$ .

In summary, two asymmetric thioether-TFSI lithium salts were developed to overcome key limitations of conventional **LiTFSI**-based PEO electrolytes. Their low melting points suppress PEO crystallinity, enabling effective plasticization while maintaining ionic conductivity and  $\text{Li}^+$  transference number. Notably, both salts suppress aluminum current-collector corrosion through formation of a stable passivation layer. When incorporated into PEO-based SPEs, these features provide improved compatibility with lithium metal and stable long-term cycling in  $\text{Li}$   $\text{LiFePO}_4$  cells with high capacity retention and Coulombic efficiency. The modular thiol-ene synthesis further enables structural tunability with reduced fluorine content, supporting scalability and regulatory compliance.

## Acknowledgements

View Article Online

DOI: 10.1039/D6CC00051G

This work was supported by Luxembourg National Research Fund (FNR) through FNRS-FNR project INFINITE (agreement no. INTER/FNRS/21/16555380/INFINITE), by the National Recovery and Resilience Plan under Next-GenerationEU (PIANO NAZIONALE DI RIPRESA E RESIL- IENZA – PNRR Mission 4, Component 2, Investment 1.4 and D.D. 1033 June 17, 2022 of the Ministero dell'Universit'a e della Ricerca (MUR), CN00000023) and by the Italian Ministry of University and Research (MUR) through the "Dipartimenti di Eccellenza 2023–2027" (CUPE17G22001490006) program.

## Data availability

The following supporting data: materials and methods; full experimental details for the synthesis of **Li TFT-TFSI** and **Li MET-TFSI**, their  $^1\text{H}$ ,  $^{13}\text{C}$ ,  $^{19}\text{F}$ , HSQC and HMBC NMR spectra, elemental analysis and DSC traces; synthesis of **Li MET-TFSI/PEO** and **Li TFT-TFSI/PEO** materials, their DSC traces, EIS and polarization current curves; anodic dissolution behavior of aluminum in 1 M  $\text{Li}$  salt in EC-DMC (1:1 v/v) liquid electrolytes; XPS analysis of aluminium disks after dissolution, specific capacity and coulombic efficiency as a function of cycle number for  $\text{Li}^0$   $\text{Li TFT-TFSI/PEO}||\text{LiFePO}_4$  and  $\text{Li}^0$   $\text{Li MET-TFSI/PEO}||\text{LiFePO}_4$  cells during galvanostatic cycling at C/15 and  $70^\circ\text{C}$  as well as their potential vs. specific capacity profiles, and critical current density tests has been provided as part of the Supplementary information. See DOI: 10.1039/x0xx00000x.

## Conflicts of interest

There are no conflicts to declare.

## Notes and references

- Z. Xue, D. He and X. Xie, *J. Mater. Chem. A*, 2015, **3**, 19218–19253.
- S. Callens, J.-F. Le Nest, A. Gandini and M. Armand, *Polym. Bull.*, 1991, **25**, 443–450.
- A. Hammami, N. Raymond and M. Armand, *Nature*, 2003, **424**, 635–636.
- J.-M. Tarascon and M. Armand, *Nature*, 2001, **414**, 359–367.
- Q. Wang, P. Ping, X. Zhao, G. Chu, J. Sun and C. Chen, *Journal of Power Sources*, 2012, **208**, 210–224.
- B. Tong, P. Wang, Q. Ma, H. Wan, H. Zhang, X. Huang, M. Armand, W. Feng, J. Nie and Z. Zhou, *Solid State Ion.*, 2020, **358**, 115519.
- L. Qiao, U. Oteo, M. Martinez-Ibañez, A. Santiago, R. Cid, E. Sanchez-Diez, E. Lobato, L. Meabe, M. Armand and H. Zhang, *Nat. Mater.*, 2022, **21**, 455–462.
- L. J. Krause, W. Lamanna, J. Summerfield, M. Engle, G. Korba, R. Loch and R. Atanasoski, *J. Power Sources*, 1997, **68**, 320–325.
- G. Guzmán-González, M. Alvarez-Tirado, J. L. Olmedo-Martínez, M. L. Picchio, N. Casado, M. Forsyth and D. Mecerreyes, *Adv. Energy Mater.*, 2023, **13**, 2202974.
- D. Flachard, J. Rolland, M. M. Obadia, A. Sergej, R. Bouchet and E. Drockenmuller, *Chem. Commun.*, 2018, **54**, 9035–9038.
- M. B. Herath, S. E. Creager, R. V. Rajagopal, O. E. Geiculescu and D. D. DesMarteau, *Electrochim. Acta*, 2009, **54**, 5877–5883.



- 12 S. Bhowmick, M. Ahmed, A. Filippov, L. C. Loaiza, F. U. Shah and P. Johansson, *Chem. Commun.*, 2023, **59**, 2620–2623.
- 13 G. B. Appetecchi and S. Passerini, *J. Electrochem. Soc.*, 2002, **149**, A891.
- 14 B. Tong, Z. Song, W. Feng, J. Zhu, H. Yu, X. Huang, M. Armand, Z. Zhou and H. Zhang, *Adv. Energy Mater.*, 2023, **13**, 2204085.
- 15 F. Castiglione, M. Moreno, G. Raos, A. Famulari, A. Mele, G. B. Appetecchi and S. Passerini, *J. Phys. Chem. B*, 2009, **113**, 10750–10759.
- 16 N. Nishi, Y. Yasui, T. Uruga, H. Tanida, T. Yamada, S. Nakayama, H. Matsuoka and T. Kakiuchi, *J. Chem. Phys.*, 2010, **132**, 164705.
- 17 H. Zhang, H. Han, X. Cheng, L. Zheng, P. Cheng, W. Feng, J. Nie, M. Armand, X. Huang and Z. Zhou, *J. Power Sources*, 2015, **296**, 142–149.
- 18 H. Zhang, Z. Song, W. Yuan, W. Feng, J. Nie, M. Armand, X. Huang and Z. Zhou, *ChemElectroChem*, 2021, **8**, 1322–1328.
- 19 L. García, D. Fraile-Insagurbe, I. Serna, I. Aldalur, L. Meabe, M. Arrese-Igor, R. Cid, J. Etxabe, M. Armand and M. Martínez-Ibañez, *EEM*, 2025, e70143.
- 20 H. Zhang, U. Oteo, H. Zhu, X. Judez, M. Martínez-Ibañez, I. Aldalur, E. Sanchez-Diez, C. Li, J. Carrasco, M. Forsyth and M. Armand, *Angew. Chem. Int. Ed.*, 2019, **58**, 7829–7834.
- 21 H. Zhang, X. Cheng, Q. Ma, W. Feng, L. Zheng, J. Nie, X. Huang, M. Armand and Z. Zhou, *Electrochim. Acta*, 2016, **207**, 66–75.
- 22 H. Zhang, U. Oteo, X. Judez, G. G. Eshetu, M. Martínez-Ibañez, J. Carrasco, C. Li and M. Armand, *Joule*, 2019, **3**, 1689–1702.
- 23 H. Zhang, F. Chen, O. Lakuntza, U. Oteo, L. Qiao, M. Martínez-Ibañez, H. Zhu, J. Carrasco, M. Forsyth and M. Armand, *Angew. Chem. Int. Ed.*, 2019, **58**, 12070–12075.
- 24 M. Martínez-Ibañez, E. Sanchez-Diez, U. Oteo, I. Gracia, I. Aldalur, H. B. Eitouni, M. Joost, M. Armand and H. Zhang, *Chem. Mater.*, 2022, **34**, 3451–3460.
- 25 L. Qiao, S. Rodríguez Peña, M. Martínez-Ibañez, A. Santiago, I. Aldalur, E. Lobato, E. Sanchez-Diez, Y. Zhang, H. Manzano, H. Zhu, M. Forsyth, M. Armand, J. Carrasco and H. Zhang, *J. Am. Chem. Soc.*, 2022, **144**, 9806–9816.
- 26 M. Zhou, K. Cui, T.-S. Wang, Z. Luo, L. Chen, Y. Zheng, B. Li, B. Shi, J. Liu, J.-J. Shao, G. Zhou, S. Yang and Y.-B. He, *ACS Nano*, 2024, **18**, 26986–26996.
- 27 Z. Luo, W. Li, C. Guo, Y. Song, M. Zhou, Y. Shi, J. Xu, L. Li, B. Shi, Q. Ouyang, J.-J. Shao and G. Zhou, *Particuology*, 2024, **85**, 146–154.
- 28 Y. V. Shevtsov, D. R. Nosov, A. S. Shaplov and D. F. Schmidt, LU601870 TFSI-functional thioether compounds for electrochemical applications, 2025.
- 29 H. T. Ho, M. Rollet, T. N. T. Phan and D. Gigmès, *Eur. Polym. J.*, 2018, **107**, 74–81.
- 30 X. Yang, M. Jiang, X. Gao, D. Bao, Q. Sun, N. Holmes, H. Duan, S. Mukherjee, K. Adair, C. Zhao, J. Liang, W. Li, J. Li, Y. Liu, H. Huang, L. Zhang, S. Lu, Q. Lu, R. Li, C. V. Singh and X. Sun, *Energy Environ. Sci.*, 2020, **13**, 1318–1325.
- 31 S. Porporato, J. L. Gómez-Urbano, A. Piovano, G. A. Elia, C. Gerbaldi and A. Balducci, *Electrochim. Acta*, 2025, **525**, 146096.
- 32 R.-S. Kühnel, M. Lübke, M. Winter, S. Passerini and A. Balducci, *J. Power Sources*, 2012, **214**, 178–184.

View Article Online  
DOI: 10.1039/D6CC00051G



**Data availability statement for**View Article Online  
DOI: 10.1039/D6CC00051G**Low Melting Non-corrosive Asymmetric Thioether-TFSI Li Salts for Solid Polymer Electrolytes**

Vladislav Y. Shevtsov<sup>a,b</sup>, Francesco Gambino<sup>c,d</sup>, Daniil R. Nosov<sup>a</sup>, Jérôme Guillot<sup>e</sup>, Silvia Porporato<sup>c,d</sup>,  
Giuseppe A. Elia<sup>c,d</sup>, Claudio Gerbaldi<sup>c,d\*</sup>, Alexander S. Shaplov<sup>a\*</sup>

<sup>a</sup> *Functional Polymeric and Particulate Materials Unit, Luxembourg Institute of Science and Technology (LIST), 28 avenue des Hauts-Fourneaux, L-4362 Esch-sur-Alzette, Luxembourg*

<sup>b</sup> *Department of Physics and Materials Science, University of Luxembourg, L-4365 Esch-sur-Alzette, Luxembourg*

<sup>c</sup> *GAME Lab, Department of Applied Science and Technology (DISAT), Politecnico di Torino, 24 Corso Duca degli Abruzzi, 10129 Torino, Italy*

<sup>d</sup> *National Reference Center for Electrochemical Energy Storage (GISEL), 9 Via G. Giusti, 50121 Firenze, Italy*

<sup>e</sup> *Advanced Analyses and Support Unit, Luxembourg Institute of Science and Technology (LIST), 28 avenue des Hauts-Fourneaux, L-4362 Esch-sur-Alzette, Luxembourg*

Correspondence:

Email: [claudio.gerbaldi@polito.it](mailto:claudio.gerbaldi@polito.it)

Email: [alexander.shaplov@list.lu](mailto:alexander.shaplov@list.lu),

The following supporting data: materials and methods; full experimental details for the synthesis of **Li TFT-TFSI** and **Li MET-TFSI**, their <sup>1</sup>H, <sup>13</sup>C, <sup>19</sup>F, HSQC and HMBC NMR spectra, elemental analysis and DSC traces; synthesis of **Li MET-TFSI/PEO** and **Li TFT-TFSI/PEO** materials, their DSC traces, EIS and polarization current curves; anodic dissolution behavior of aluminum in 1 M **Li salt** in EC-DMC (1:1 v/v)



liquid electrolytes; specific capacity and coulombic efficiency as a function of cycle number for  $\text{Li}^\circ\|\text{Li TFSI-TFSI/PEO}\|\text{LiFePO}_4$  and  $\text{Li}^\circ\|\text{Li MET-TFSI/PEO}\|\text{LiFePO}_4$  cells during galvanostatic cycling at C/15 and 70 °C as well as their potential vs. specific capacity profiles, has been provided as part of the Supplementary information. See DOI: 10.1039/x0xx00000x.

View Article Online

DOI: 10.1039/D6CC00051G

